

# Phonon transport of three-fold degeneracy topological semimetal MoP

San-Dong Guo

*School of Physics, China University of Mining and Technology, Xuzhou 221116, Jiangsu, China*

Recently, three-component new fermions in topological semimetal MoP are experimentally observed, which may have potential applications like topological qubits, low-power electronics and spintronics. These are closely related to thermal transport properties of MoP. In this work, the phonon transport of MoP is investigated by solving the linearized phonon Boltzmann equation within the single-mode relaxation time approximation (RTA). The calculated room-temperature lattice thermal conductivity is  $18.41 \text{ Wm}^{-1}\text{K}^{-1}$  and  $34.71 \text{ Wm}^{-1}\text{K}^{-1}$  along the in- and cross-plane directions, exhibiting very strong anisotropy. The isotope and size effects on the lattice thermal conductivity are also considered. It is found that isotope scattering produces little effect, and phonon has little contribution to the lattice thermal conductivity, when phonon mean free path(MFP) is larger than  $0.15 \mu\text{m}$  at 300 K. It is noted that average room-temperature lattice thermal conductivity of MoP is lower than that of representative Weyl semimetal TaAs, which is due to smaller group velocities and larger Grüneisen parameters. Our works provide valuable informations for the thermal management of MoP-based nano-electronics devices, and motivate further experimental works to study thermal transport of MoP.

PACS numbers: 72.15.Jf, 71.20.-b, 71.70.Ej, 79.10.-n

Email:guosd@cumt.edu.cn

Keywords: Lattice thermal conductivity; Group velocities; Phonon lifetimes

## I. INTRODUCTION

The study of new type of topological nontrivial phase, from topological insulator to semimetal, has attracted great research interest in recent years<sup>1-9</sup>. Dirac semimetals, Weyl semimetals and nodal line semimetals are three kinds of representative topological semimetals<sup>4,5,9</sup>. By including the spin-orbit coupling (SOC) or mass term, the nodal line structure can turn into Weyl points, Dirac points or a topological insulator<sup>10</sup>. The  $\text{Na}_3\text{Bi}$  is a classic Dirac Semimetal, which has been confirmed by angle-resolved photoemission spectroscopy (ARPES), and three-dimensional (3D) Dirac fermions with linear dispersions have been detected along all momentum directions<sup>6</sup>. The first experimental realization of a Weyl semimetal is in TaAs, and both the Weyl fermions and Fermi arc surface states have been detected<sup>4</sup>, which has been further confirmed by ARPES<sup>11</sup>. Both Weyl and Dirac fermions are even-component, which are two- and four-component, respectively. Recently, three-component fermions have been predicted in ZrTe with the WC-structure by first-principles calculations<sup>12</sup>. Then, a triply degenerate point in MoP with the WC-structure has been detected by ARPES, and pairs of Weyl points coexist with the three-component fermions<sup>8</sup>.

Most studies focus on the topological electronic structure of these exotic materials, but little research can be found to investigate the thermal transport in these topological semimetals. As is well known, the thermal transport property is closely related to the application of a material in nano-devices. Recently, thermal transport in TaAs has been investigated from a first principles calculation, and the lattice thermal conductivity shows obvious anisotropy along the a(b) and c crystal axis<sup>13</sup>. The thermoelectric properties of TaAs have also been investigated, and the maximum thermoelectric figure of

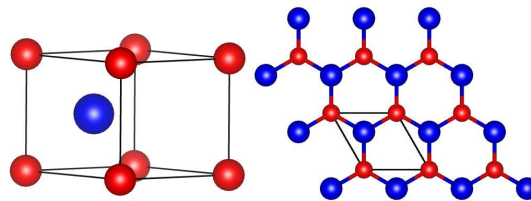


FIG. 1. (Color online) The crystal structure of MoP in one unit cell, and top view of the crystal structure. The blue and red balls represent Mo and P atoms, respectively.

merit  $ZT$  reaches up to 0.63 at 900 K in n-doping along c crystal axis<sup>14</sup>. Here, the phonon transport properties of three-fold degeneracy topological semimetal MoP are investigated by solving the phonon Boltzmann transport equation. The lattice thermal conductivity is predicted, and the isotope and size effects on the lattice thermal conductivity are also studied. The lattice thermal conductivity shows a distinct anisotropic property along the a(b) and c crystal axis. The phonon mode group velocities, lifetimes and Grüneisen parameters are calculated to understand deeply the phonon transport of MoP.

The rest of the paper is organized as follows. In the next section, we shall give our computational details. In the third section, we shall present phonon transport of MoP. Finally, we shall give our conclusions in the fourth section.

## II. COMPUTATIONAL DETAIL

First-principles calculations are performed within the projected augmented wave (PAW) method, and the exchange-correlation energy functional of generalized gradient approximation of the Perdew-Burke-Ernzerhof

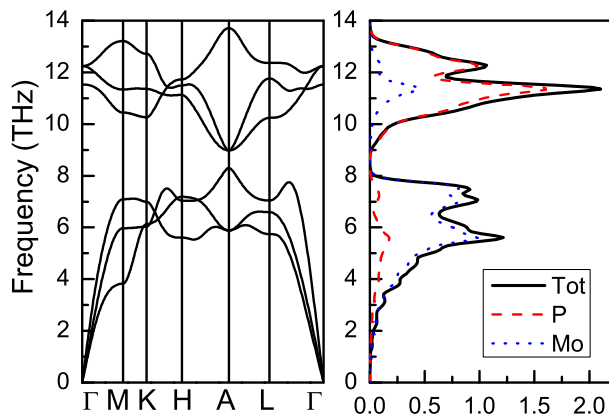


FIG. 2. (Color online) Phonon band structures of MoP with the corresponding total density of states (DOS) and atom partial DOS (PDOS).

(GGA-PBE) is adopted, as implemented in the VASP code<sup>15–18</sup>. A plane-wave basis set is employed with kinetic energy cutoff of 400 eV, and the  $s^2p^3$  orbitals of P and  $4p5s4d$  orbitals of Mo are treated as valance ones. The electronic stopping criterion is  $10^{-8}$  eV. The lattice thermal conductivity of MoP is carried out by solving linearized phonon Boltzmann equation with the single mode RTA, as implemented in the Phono3py code<sup>19</sup>. The interatomic force constants (IFCs) are calculated by the finite displacement method. The second-order harmonic IFCs are calculated using a  $4 \times 4 \times 4$  supercell containing 128 atoms with k-point meshes of  $2 \times 2 \times 2$ . Using the harmonic IFCs, phonon dispersion of MoP can be calculated by Phonopy package<sup>20</sup>. The phonon dispersion determines the allowed three-phonon scattering processes, and further the group velocity and specific heat can be attained. The third-order anharmonic IFCs are calculated using a  $3 \times 3 \times 3$  supercells containing 54 atoms with k-point meshes of  $3 \times 3 \times 3$ . Based on third-order anharmonic IFCs, the three-phonon scattering rate can be calculated, and further the phonon lifetimes can be attained. To compute lattice thermal conductivities, the reciprocal spaces of the primitive cells are sampled using the  $20 \times 20 \times 20$  meshes.

### III. MAIN CALCULATED RESULTS AND ANALYSIS

As shown in Figure 1, MoP possesses WC-type crystal structure with space group  $P\bar{6}m2$  (No. 187), where Mo and P atoms occupy the 1d ( $1/3, 2/3, 1/2$ ) and 1a (0,0,0) Wyckoff positions, respectively. The experimental lattice constants ( $a=b=3.231$  Å,  $c=3.207$  Å) are used to investigate elastic properties and phonon transport of MoP<sup>21</sup>. The five independent elastic constants  $C_{ij}$  are calculated, and the corresponding values (in GPa):  $C_{11}=359.00$ ,  $C_{12}=153.73$ ,  $C_{13}=160.14$ ,  $C_{33}=515.15$  and  $C_{44}=169.22$ . The hexagonal mechanical stability criteria are given

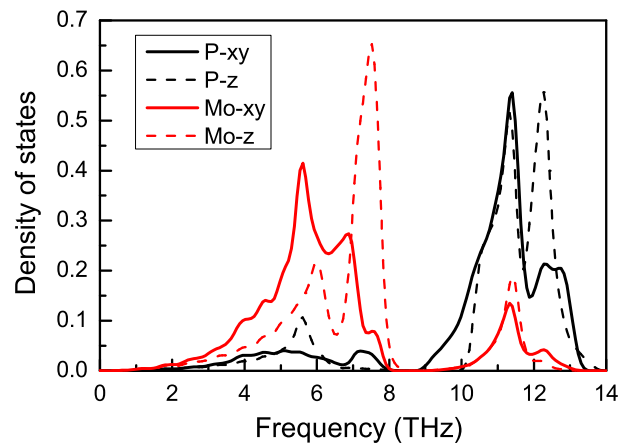


FIG. 3. (Color online) The x(y) and z components of atom PDOS of MoP.

by<sup>22</sup>:  $C_{44} > 0$ ,  $C_{11} > |C_{12}|$  and  $(C_{11} + 2C_{12})C_{33} > 2C_{13}^2$ . By simple calculation, these criteria are satisfied for MoP, proving mechanical stability of MoP. Based on elastic constants  $C_{ij}$ , the bulk ( $B$ ), shear ( $G$ ), and Young ( $E_{xx}$  and  $E_{zz}$ ) moduli (in GPa) are 239.10, 134.96, 274.28 and 415.11, respectively.

Based on the eigenvalues of harmonic IFCs matrix, the phonon dispersion of MoP along several high symmetry paths is obtained. The phonon dispersion along with total and atom partial density of states (DOS) are plotted in Figure 2. It is clearly seen that no imaginary frequencies are produced in the phonon dispersion of MoP, which indicates the thermodynamic stability of MoP. There are 3 acoustic and 3 optical phonon branches because of two atoms per unit cell. It can be noted that there is a phonon band gap of 0.68 THz, separating acoustic branches from optical branches. The phonon band gap may be due to different atomic masses of P and Mo atoms<sup>23,24</sup>. From atom partial DOS, acoustic (optical) branches are mainly contributed by the vibrations of Mo (P) atoms. According to Figure 3, the x(y) modes of P and Mo atoms have stronger coupling with the z modes in high frequency region than in low frequency region. As is well known, the phonons in the low frequency region dominate the lattice thermal conductivity. Therefore, the weak coupling between x(y) and z modes may lead to strong anisotropy of lattice thermal conductivity along a(b) and c directions.

Based on harmonic and anharmonic IFCs, the intrinsic lattice thermal conductivity of MoP is calculated by solving the linearized phonon Boltzmann equation within single-mode RTA method. The lattice thermal conductivities of infinite (Pure) MoP along a(b) and c directions as a function of temperature are plotted in Figure 4. In the considered temperature region, the lattice thermal conductivity of MoP decreases with increasing temperature, which is due to intrinsic enhancement of phonon-phonon scattering. It is found that the lattice thermal conductivity exhibits obvious anisotropy, in which the lattice thermal conductivity along c direction was higher

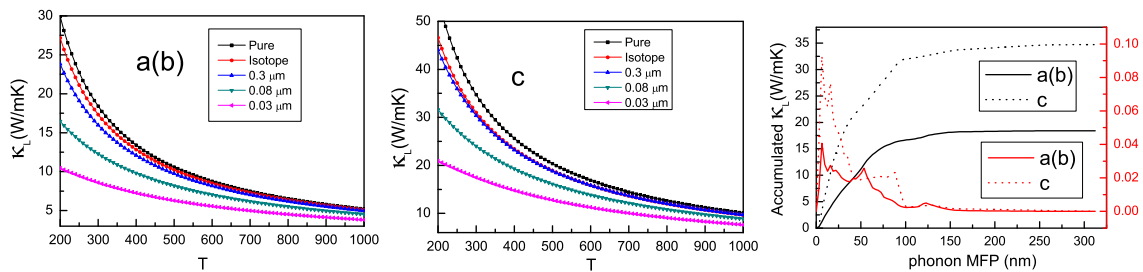


FIG. 4. (Color online) The lattice thermal conductivities of infinite (Pure and Isotope) and finite-size (0.3, 0.08 and 0.03  $\mu\text{m}$ ) MoP as a function of temperature, including a(b) and c directions; The cumulative lattice thermal conductivity (300 K) of infinite (Pure) MoP with respect to phonon mean free path, and the derivatives.

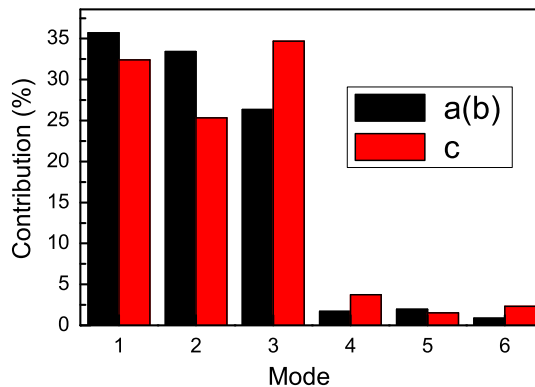


FIG. 5. (Color online) The phonon modes contributions along a(b) and c directions to total lattice thermal conductivity at room temperature. 1, 2, 3 represent TA1, TA2 and LA branches and 4, 5, 6 for optical branches.

than that along a(b) direction. The room-temperature lattice thermal conductivities of infinite (Pure) MoP along a(b) and c directions are  $18.41 \text{ Wm}^{-1}\text{K}^{-1}$  and  $34.71 \text{ Wm}^{-1}\text{K}^{-1}$ , respectively. An anisotropy factor<sup>13</sup>, defined as  $\eta = (\kappa_L(cc) - \kappa_L(aa))/\kappa_L(aa)$ , is used to measure the anisotropic strength, and the corresponding value is 88.5%. The lattice thermal conductivity is related to Young's modulus by  $\kappa_L \sim \sqrt{E}$ <sup>25</sup>. It is found that the Young's modulus along a(b) direction is smaller than that along c direction, which is identical with that of lattice thermal conductivity.

Next, we consider phonon-isotope scattering and boundary scattering. Based on the formula proposed by Shin-ichiro Tamura<sup>26</sup>, the phonon-isotope scattering is calculated. For boundary scattering, the scattering rate can be simply calculated by  $v_g/L$ , in which  $v_g$ ,  $L$  are the group velocity and the boundary mean free path, respectively. The lattice thermal conductivities of infinite (Isotope) and finite-size (0.3, 0.08 and 0.03  $\mu\text{m}$ ) MoP as a function of temperature are shown in Figure 4. At 300 K, the lattice thermal conductivities along a(b) and c directions are  $17.34 \text{ Wm}^{-1}\text{K}^{-1}$  and  $31.01 \text{ Wm}^{-1}\text{K}^{-1}$  for infinite (Isotope) MoP, which are slightly lower than those of infinite (Pure) MoP. With the sample size decreasing, it is clearly seen that the lattice thermal con-

ductivity decreases because of enhanced boundary scattering. For the 0.3, 0.08 and 0.03  $\mu\text{m}$  cases, at room temperature, the lattice thermal conductivity is reduced by about 13.25%, 33.27% and 53.31% with respect to that of infinite (pure) case along a(b) direction, and 12.47%, 30.79% and 49.63% along c direction. The contribution to total lattice thermal conductivity from individual phonon modes with different MFP can predict the size effect, because it shows how phonons with different MFP contribute to the thermal conductivity. The cumulative lattice thermal conductivity along with the derivatives with respect to MFP (300 K) along a(b) and c directions are shown in Figure 4. It is clearly seen that the cumulative lattice thermal conductivity along both a(b) and c directions approaches saturation value with MFP increasing. Phonons with MFP larger than 0.15  $\mu\text{m}$  only lightly contribute to the lattice thermal conductivity. Phonons with MFP smaller than 0.04  $\mu\text{m}$  along a(b) direction and 0.03  $\mu\text{m}$  along z direction contribute around half to the lattice thermal conductivity. According to the derivatives, phonons dominating the lattice thermal conductivity along c direction have shorter MFP than ones along a(b) direction.

At room temperature, the phonon modes contributions along a(b) and c directions to the total lattice thermal conductivity are plotted in Figure 5. It is evident that the acoustic phonon modes dominate the lattice thermal conductivity of MoP, while the contribution from the optical branches is quite small. The acoustic branches provide a contribution of 95.48% along a(b) direction and 92.41% along c direction. Along a(b) direction, any of two transverse acoustic phonon modes (TA1 or TA2) has larger contribution than longitudinal acoustic phonon mode (LA), while LA provides larger contribution than TA1 or TA2 along c direction. To gain more insight into phonon transport of MoP, the mode level phonon group velocities and lifetimes are plotted in Figure 6. The largest group velocities of TA1 and TA2 branches near  $\Gamma$  point are almost the same, and the corresponding value is  $4.68 \text{ kms}^{-1}$ . It is  $6.95 \text{ kms}^{-1}$  for the largest group velocity of LA branch near  $\Gamma$  point. The most of group velocities of LA branch are larger than those of TA2 and TA1 branches, while the smallest group velocities are observed for the TA1 branch. It can be noted

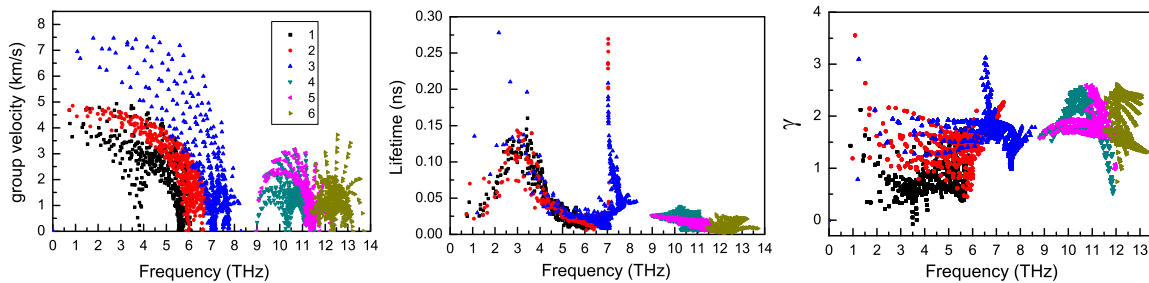


FIG. 6. The mode level phonon group velocities, phonon lifetimes (300K) and Grüneisen parameters of infinite (Pure) MoP in the first Brillouin zone. 1, 2, 3 represent TA1, TA2 and LA branches and 4, 5, 6 for optical branches.

that the most of group velocities of acoustic branches are higher than those of optical branches. It is found that most of phonon lifetimes of three acoustic branches overlap below about 6.5 THz. Unexpectedly, the phonon lifetimes of TA2 and LA near 7.5 THz become large. It is also noted that most of phonon lifetimes of three acoustic phonon modes are larger than those of optical branches. Together with their large group velocities, these results lead to the dominant contribution from the three acoustic phonon modes to the total lattice thermal conductivity. Mode Grüneisen parameters can provide information about anharmonic interactions, determining the intrinsic phonon-phonon scattering, and can be attained directly from the third order anharmonic IFCs. The mode level Grüneisen parameters of infinite (Pure) MoP are shown in Figure 6. The large  $\gamma$  is in favour of low lattice thermal conductivity because of strong anharmonicity. For TA2, LA and optical branches, the  $\gamma$  is fully positive. However, TA1 branch has a small negative  $\gamma$ . The average Grüneisen parameter is 1.57, indicating relatively strong anharmonic phonon scattering.

#### IV. CONCLUSION

Phonon transport in Weyl semimetal TaAs has been investigated by combining first principle calculations and Boltzmann phonon transport equation<sup>13,14</sup>. The lattice thermal conductivity of TaAs also shows obvious anisotropy along a(b) and c directions. The room-temperature one is  $39.26 \text{ Wm}^{-1}\text{K}^{-1}$  along a(b) direction, which is larger than  $24.78 \text{ Wm}^{-1}\text{K}^{-1}$  along c direction<sup>13</sup>. This is different from that of MoP, where the lattice thermal conductivity along a(b) direction is smaller than one along c direction. It is found that the average lattice ther-

mal conductivity ( $\kappa_L(av) = (\kappa_L(aa) + \kappa_L(bb) + \kappa_L(cc))/3$ ) of MoP is smaller than that of TaAs. This can be explained by group velocities and Grüneisen parameters. Calculated results show MoP has smaller group velocities than TaAs<sup>14</sup>, which partially gives rise to lower lattice thermal conductivity for MoP than TaAs. Another factor is that MoP has larger Grüneisen parameters than TaAs<sup>14</sup>, which induces more stronger anharmonicity, leading to lower lattice thermal conductivity.

In summary, based on the first-principles calculations and semiclassical Boltzmann transport theory, we investigate the phonon transport properties of MoP, which contains three-component fermions in the bulk electronic structure. The lattice thermal conductivity of MoP shows an obvious anisotropy, and the room-temperature lattice thermal conductivity is  $18.41 \text{ Wm}^{-1}\text{K}^{-1}$  and  $34.71 \text{ Wm}^{-1}\text{K}^{-1}$  along the a(b) and c crystal axis, respectively. For designing nanostructures, the size dependence of lattice thermal conductivity is investigated, and phonons with MFP larger than  $0.15 \mu\text{m}$  have little contribution to the total lattice thermal conductivity. The lower lattice thermal conductivity of MoP than TaAs can be understood by lower group velocities and larger Grüneisen parameters. Our works shed light on phonon transport of MoP, and will motivate farther experimental studies of thermal transport properties of topological semimetals.

#### ACKNOWLEDGMENTS

This work is supported by the National Natural Science Foundation of China (Grant No.11404391). We are grateful to the Advanced Analysis and Computation Center of CUMT for the award of CPU hours to accomplish this work.

<sup>1</sup> H. J. Zhang, C. X. Liu, X. L. Qi, X. Dai, Z. Fang and S. C. Zhang, Nat. Phys. **5**, 438 (2009).

<sup>2</sup> X. L. Qi and S. C. Zhang, Rev. Mod. Phys. **83**, 1057 (2011).

<sup>3</sup> M. Z. Hasan and C. L. Kane, Rev. Mod. Phys. **82**, 3045

(2010).

<sup>4</sup> B.Q. Lv, H. M. Weng, B. B. Fu, X. P. Wang, H. Miao, J. Ma, P. Richard, X. C. Huang, L. X. Zhao, G. F. Chen, Z. Fang, X. Dai, T. Qian, and H. Ding, Phys. Rev. X **5**,

- 031013 (2015).
- <sup>5</sup> Z. J. Wang, Y. Sun, X. Q. Chen, C. Franchini, G. Xu, H. M. Weng, X. Dai, and Z. Fang, *Phys. Rev. B* **85**, 195320 (2012)
- <sup>6</sup> Z. K. Liu, B. Zhou and Y. Zhang et al., *Science* **343**, 864 (2014).
- <sup>7</sup> R. M. Lutchyn, J. D. Sau, and S. D. Sarma, *Phys. Rev. Lett.* **105**, 077001 (2010).
- <sup>8</sup> B. Q. Lv, Z. L. Feng, Q.-N. Xu et al., *Nature* **546**, 627 (2017).
- <sup>9</sup> C. Fang, H. M. Weng, X. Dai and Z. Fang, *Chinese Phys. B* **25**, 117106 (2016).
- <sup>10</sup> R. Yu, Z. Fang, X. Dai, H. M. Weng, *Front. Phys.* **12**, 127202 (2017)
- <sup>11</sup> L. X. Yang, Z. K. Liu and Y. Sun et al., *Nat. Phys.* **11**, 728 (2015).
- <sup>12</sup> H. Weng, C. Fang, Z. Fang, and X. Dai, *Phys. Rev. B* **94**, 165201 (2016).
- <sup>13</sup> T. Ouyang, H. P. Xiao, C. Tang, M. Hu and J. X. Zhong, *Phys. Chem. Chem. Phys.* **18**, 16709 (2016).
- <sup>14</sup> B. Peng, H. Zhang, H. Z. Shao, H. L. Lu, D. W. Zhang, H. Y. Zhua, *Nano Energy* **30**, 225 (2016).
- <sup>15</sup> G. Kresse, *J. Non-Cryst. Solids* **193**, 222 (1995).
- <sup>16</sup> G. Kresse and J. Furthmüller, *Comput. Mater. Sci.* **6**, **15** (1996).
- <sup>17</sup> J. P. Perdew, K. Burke and M. Ernzerhof, *Phys. Rev. Lett.* **77**, 3865 (1996).
- <sup>18</sup> G. Kresse and D. Joubert, *Phys. Rev. B* **59**, 1758 (1999).
- <sup>19</sup> A. Togo, L. Chaput and I. Tanaka, *Phys. Rev. B* **91**, 094306 (2015).
- <sup>20</sup> A. Togo, F. Oba, and I. Tanaka, *Phys. Rev. B* **78**, 134106 (2008).
- <sup>21</sup> The experimental lattice constants are attained from the Inorganic Crystal Structure Database (ICSD).
- <sup>22</sup> Z. J. Wu, E. J. Zhao, H. P. Xiang, X. F. Hao, X. J. Liu and J. Meng, **76**, 054115 (2007).
- <sup>23</sup> L. Lindsay, D. A. Broido and T. L. Reinecke, *Phys. Rev. Lett.* **111**, 025901 (2013).
- <sup>24</sup> X. Gu and R. Yang, *Appl. Phys. Lett.* **105**, 131903 (2014).
- <sup>25</sup> W. Kim, *J. Mater. Chem. C* **3**, 10336 (2015).
- <sup>26</sup> S.I. Tamura, *Phys. Rev. B*, **27**, 858 (1983).